The International Journal of Advanced Manufacturing Technology (2024) 132:6019–6031
https://doi.org/10.1007/s00170-024-13694-6

ORIGINAL ARTICLE

Field-assisted sintering of high-entropy alloy-reinforced aluminium matrix composites: phase identification and microstructural properties

Smith Salifu[1] · **Peter Apata Olubambi**[1]

Received: 20 January 2024 / Accepted: 25 April 2024 / Published online: 8 May 2024

Abstract
This study investigates the design, phase identification, and microstructural properties of high-entropy alloy (HEA)-reinforced aluminium (Al) matrix composites. Thermophysical expressions for HEAs were employed during the design phase of the HEA; both theoretical frameworks and experimental analyses were used to anticipate stable phases while a field-assisted sintering technique was employed to consolidate the samples. Calculation of phase diagram (CALPHAD) predictions for the phases present in the HEA align with valence electron concentration (VEC) calculations as both predicted the presence of BCC and FCC phases. The microhardness results reveal a substantial increase in the hardness value of the composites as compared to the pure Al, such that as low as 5 wt% HEA addition resulted in over a 100% improvement, while the densification of the composites was found to decrease with an increase in the wt% of HEA. SEM micrographs and XRD analyses show fair dispersion, bonding, and phase integration in the HEA-reinforced composites.

Keywords Field-assisted sintering · High-entropy alloy · Aluminium matrix composites · Phases · Microhardness · Interdiffusion

1 Introduction

In recent years, the field of materials science and engineering has experienced significant strides, leading to the development of innovative materials tailored for diverse applications [1]. Among these materials, the integration of high-entropy alloys (HEAs) into metal matrix composites (MMCs) has garnered considerable attention, offering unique properties that set them apart from conventional alloys [2]. HEAs are characterized by a composition of multiple principal elements; thus, they exhibit exceptional mechanical, thermal, and corrosion-resistant properties which make them promising candidates for various engineering applications [2, 3]. Furthermore, MMCs, consisting of a metallic matrix reinforced with a secondary phase, have gained widespread recognition due to their enhanced properties, which include improved strength, stiffness, wear resistance, and thermal performance [4, 5].

The synergy between aluminium matrix and HEA reinforcement has emerged as a particularly intriguing avenue, demonstrating substantial improvements in the mechanical properties of aluminium matrix composites (AMCs) [6, 7]. Previous studies have employed various fabrication techniques such as mechanical alloying [8], fusion stir processing [9], and spark plasma sintering (SPS) [10] to consolidate HEA-reinforced aluminium matrix composites, with enhanced strength and plasticity.

Owning to the fact that the utilization of HEAs as special reinforcements for aluminium matrices has gained significant attention [11–13], Chen et al. [8] successfully employed AlCoNiCrFe HEA to reinforce pure aluminium matrix through mechanical alloying, and the addition of HEA to the aluminium matrix resulted in increased tensile strength of the AMCs. Li et al. [9] used AlCoCrFeNi HEA to reinforce AA5083 aluminium plates, and the reinforced AMCs showcased substantial enhancements in mechanical properties compared to the base aluminium matrix. Additionally, Tan et al. [10] utilized spark plasma sintering (SPS) to consolidate Al0.6CoCrFeNi particles, and the developed

✉ Smith Salifu
smithsalifu@gmail.com

[1] Centre for Nanoengineering and Advanced Materials, University of Johannesburg, Johannesburg, South Africa

Al-based amorphous composites displayed a high compressive yield strength.

Various fabrication techniques have been explored to incorporate HEAs into metal matrix, and each of the techniques used has its uniqueness in terms of influencing the mechanical and microstructural properties of the developed MMCs. Liu et al. [14] employed the SPS technique to fabricate aluminium matrix-reinforced AlCoCrFeNi HEA particles, and the outcome of the study revealed that there is a correlation between sintering temperature, interfacial layer thickness, and improved plasticity. Vacuum hot pressing, as demonstrated by Chen et al. [15], was employed to prepare AlCoNiCrFe HEA particles reinforced copper matrix, and the fabricated MMCs demonstrated a notable increase in yield strength. Wang et al. [11] utilized rotation friction extrusion (RFE) in the fabrication of CrMnFeCoNi HEA-reinforced Al matrix composites. During this process, the HEA particles reacted with the Al matrix, forming numerous FCC phases and substantially enhancing the tensile strength of the resulting AMCs.

Although the focus of this study is on AMC studies, exploring the application of HEA-reinforced metal composites extends beyond aluminium matrix. The addition of 20 wt% AlCoNiCrFe HEA to copper matrix resulted in a remarkable 220% increase in compressive strength [15]. Additionally, SPS was employed to consolidate Al0.6CoCrFeNi HEA particle-reinforced aluminium-based composites, and the developed AMCs displayed high fracture strength in the range of 3120 ± 80 MPa [10]. Comparison studies have highlighted the superiority of HEA-reinforced Al matrix composites over traditional composites, as they often showcase higher tensile strength, modulus of elasticity, and improved plasticity [16]. Furthermore, previous research indicates that composites consolidated via spark plasma sintering exhibit superior mechanical properties and excellent corrosion resistance [17]. Praveen et al. [18] explored stir casting to incorporate a cast-manufactured Al-20Cu-10Mg HEA into a 2024 aluminium alloy matrix, resulting in substantial improvements in mechanical properties. When 15% HEAs were added to the 2024 aluminium alloy, yield strength increased 1.95 times, and tensile strength improved about 1.7 times.

In this study, we leverage the promising material paradigms of aluminium matrix and high-entropy alloys (HEAs) whose composition is carefully determined through the use of novel thermophysical expressions and the calculation phase diagram (CALPHAD) prediction approach, to develop a field-assisted sintered HEA-reinforced Al matrix composites, with a focus on phase identification and microstructural properties. By employing advanced techniques such as field-assisted sintering, the study aims to contribute to the understanding of the unique combination of aluminium and HEAs, thus offering insights into the potential for fabricating lightweight, high-performance metal matrix composites with applications in various engineering sectors.

2 Methodology

The synthesis of Al matrix composites reinforced with CuNbMnCrNiCo high-entropy alloy (HEA) involved a well-defined fabrication process utilizing field-assisted sintering. This methodology encompassed powder preparation, milling/mixing, field-assisted or spark plasma sintering (SPS), and subsequent characterization. During the design of the HEA reinforcement for the aluminium matrix composites, we employed thermophysical parameter expressions to guide the selection of constituent elements. Additionally, the calculation phase diagram (CALPHAD) software, Thermocalc, was utilized to predict the potential phases present in the HEA (details in Section 3.1).

2.1 Thermophysical expression for HEA design and phase identification

In the realm of designing high-entropy alloys (HEAs), the precise anticipation of stable phases plays a pivotal role in discerning their potential applications [19]. Researchers, such as Yang [20] and Guo et al. [21, 22], have devised mechanisms aimed at favouring the formation of stable phases, including body-centered cubic (BCC), face-centered cubic (FCC), or a combination of both. The expressions formulated by these authors serve as crucial tools in predicting the stable phases during the development of HEAs. Table 1 encapsulates these expressions for determining stable phases, and these expressions are used in this study to predict the values and phases specific to the CuNbMnCrNiCo HEA developed in the current study.

The table not only provides insights into the theoretical framework employed for predicting phases but also furnishes valuable data on the anticipated phases for the HEA under investigation. This predictive approach aids in understanding the potential microstructure of the alloy, paving the way for informed decisions regarding its applications. By leveraging the expertise outlined by Yang and Guo et al. [21, 22], researchers can navigate the complex landscape of phase stability in HEAs, allowing for tailored alloy designs with desirable microstructural attributes. The synergy between theoretical predictions and experimental validations, as encapsulated in Table 1, forms a cornerstone in advancing the development and application of high-entropy alloys.

2.2 Powder preparation

Commercial spherical aluminium powder (99.8% purity) served as the matrix material, while high-purity Cu, Nb, Mn,

Table 1 Thermophysical expressions used for the determination of HEA phase stability

S/*N*	Expressions	Parameters	Remarks
1	$\Omega = \frac{T_m \Delta S_{mix}}{\Delta H_{mix}}$	T_m represents the melting temperature, ΔS_{mix} corresponds to mixing entropy, and ΔH_{mix} denotes mixing enthalpy	The requirement for the formation of a solid solution HEA is that Ω should exceed or be equal to 1.10 ($\Omega \geq 1.10$)
2	$\delta = \sqrt{\sum_{i=1}^{n} \left(c_i\left(1 - r_i / \bar{r}\right)\right)^2}$	c_i represents the atomic ratio of the ith element, r_i denotes the atomic radius of the ith element, and r represents the average atomic radius, where n stands for the total number of elements constituting the HEA	To facilitate the creation of a solid solution high-entropy alloy (HEA), it is essential that $\delta \leq 6.6\%$ [21]
3	$\Delta H_{mix} = \sum_{i=1, i\neq j}^{n} 4\Delta H_{ij}^{mix} c_i c_j$	ΔH_{ij}^{mix} represents the mixing enthalpy between the ith and jth elements	The HEA is stable if $-15 < \Delta H_{mix} < 5kJ/mol$ [23, 24]
4	$T_{mix} = \sum_{i=1}^{n} c_i \left(T_m\right)_i$	The symbol $\left(T_m\right)_i$ denotes the melting point of the ith element	T_{mix} represents the anticipated melting temperature of the HEA
5	$\Delta S_{mix} = -R \sum_{i=1}^{n} \left(c_i ln c_i\right)$	R stands for the universal gas constant, with a value of 8.314 J/K·mol	The HEA phase is stable if the condition $12 \leq \Delta S \leq 17.5$ J/K is satisfied [23, 24]
6	$VEC = \sum_{i=1}^{n} c_i (VEC)_i$	*VEC*, denoting Valence Electron Concentration, is calculated using the atomic ratio of the ith element, represented as c_i, in the HEA composed of n elements	For *VEC* values greater than or equal to 8 ($VEC \geq 8$), the stability of the FCC phase is indicated. Conversely, when VEC is less than or equal to 6.87 ($VEC \leq 6.87$), stability leans towards the BCC phase. When VEC falls within the range of 6.87 to 8 ($6.87 < VEC < 8$), both FCC and BCC phases are considered stable [25–27]

Table 2 Powder compositions for the development of HEA

Elements	Cu	Nb	Mn	Cr	Ni	Co
Atomic %	20	10	20	20	20	10

Table 3 Composition of the HEA added and pure Al used in the fabrication of the AMCs in wt%

S/*N*	HEA (wt%)	Pure Al (wt%)
1	5	95
2	7	93
3	10	90

Cr, Ni, and Co powders (each > 99%, particle size ≤ 25 µm) were utilized for the HEA reinforcement. The elemental powders for the HEA were subjected to planetary milling for 4 h at 200 RPM, intermittently paused for 10 min every 30 min. This process ensured the reduction of particle size and homogenous blending of the alloy constituents. The resulting HEA powder composition is provided in Table 2.

2.3 Mixing of HEA-reinforced Al matrix composites

The milled HEA powder was blended with the Al matrix in a turbula mixer for 24 h at a frequency of 50 Hz. Different weight percentages of HEA were mixed with pure Al, as outlined in Table 3. The 10:1 ball-to-powder ratio during milling is aimed at enhancing the homogeneity of the mixed powder.

2.4 Field-assisted sintering

Consolidation of the well-mixed HEA-reinforced Al matrix composites was accomplished through the field-assisted sintering technique also known as the spark plasma sintering (SPS) technique. A 20-mm diameter graphite die, known for its high strength and heat resistance, was employed during the sintering process, and the sintering was conducted in the field-assisted or SPS heating chamber whose schematic is shown in Fig. 1. The sintering parameters included a temperature of 520 °C, a holding time of 10 min, a sintering rate of 100 °C/min, and a sintering pressure of 50 MPa.

2.5 Field-assisted sintering profile analysis

Field-assisted sintering profile analysis for the HEA-reinforced Al matrix composite in Fig. 2 reveals insights into the between sintering time, punch displacement, and sintering temperature. The sintering profile can be delineated into five distinctive stages, with each contributing to overall densification. In the initial stage, also known as the preheating stage (0–6 min), a constant temperature of 250 °C representing the initial temperature of the furnace is maintained for 6 min while applying pressure of 50 MPa. Simultaneously, pressing gradually commences, initiating compaction. The

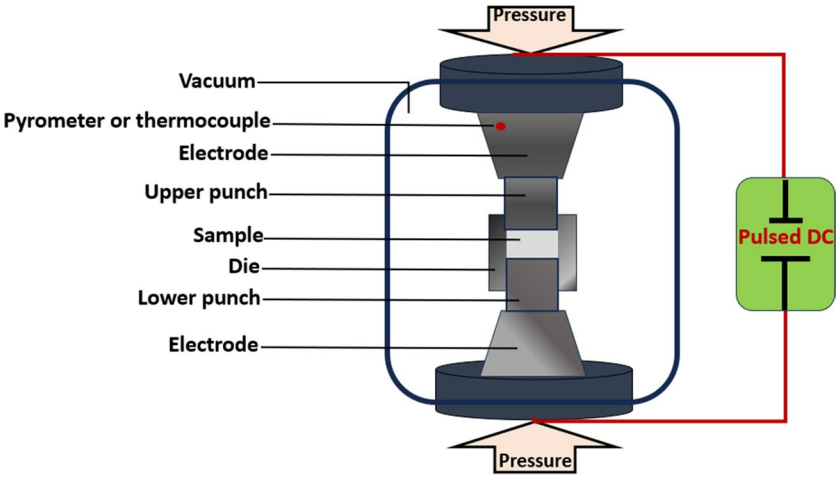

Fig. 1 Field-assisted or SPS heating chamber

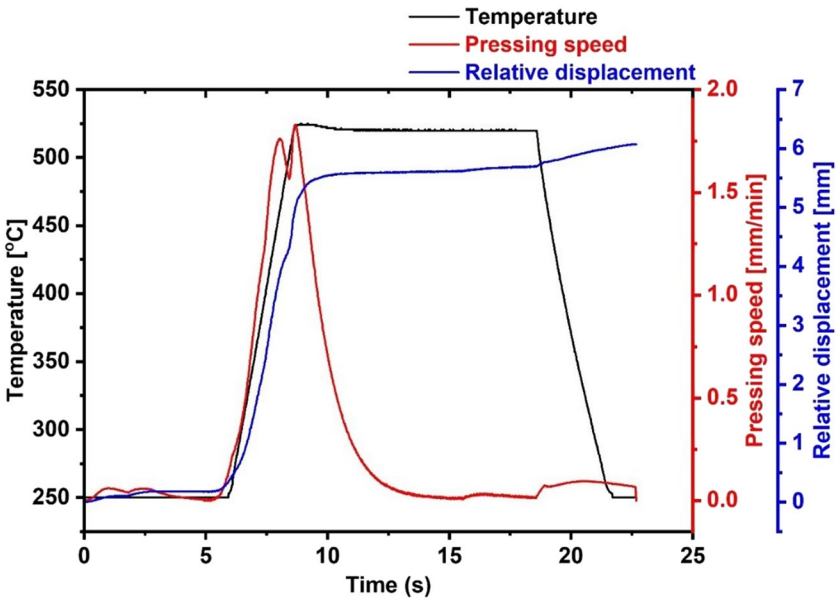

Fig. 2 Sintering profile for field-assisted sintering of HEA-reinforced Al matrix composite

punch's relative displacement slightly increases, indicating initial compaction and thermal expansion at the lower temperature. Subsequently, the heating stage (6–8 min) also known as the second stage involves a rapid temperature surge from 250 to 520 °C within 2 min with a rise in the pressing speed and displacement of the punch, and the relative displacement reflecting significant densification as the HEA reaches its sintering temperature. At the holding stage (8–18 min) also known as stage three, the heating or sintering temperature is maintained at 520 °C for 10 min, while the pressing speed gradually diminishes, stabilizing the relative displacement. This zero displacement obtained at this stage signifies full densification of the sintered sample. Stage four also known as the fast cooling stage (18–21.5 min) sees a rapid temperature decrease from 520 to 250 °C in 3.5 min with the pressing speed remaining at zero, while a slight relative displacement was observed due to thermal contraction, targeted at controlling the microstructure and minimize residual stresses in the sintered sample. Finally, the slow cooling stage (21.5–23 min) known as stage five involves a gradual temperature below 250 °C, and the stage lasts for about 1.5 min.

2.6 Characterization of samples

After the field-assisted sintering of the HEA-reinforced Al matrix composites powder, the consolidated samples were wire cut and then subjected to the appropriate metallographic operation. During the metallographic operations, the samples were etched using Keller's solution after which they underwent comprehensive characterization processes. Vicker's microhardness was determined using the INNOVATEST FALCON 500 microhardness tester, by applying a 100 gf load for 15 s. Ten different indentations were

randomly conducted on each of the samples, and the average was determined and used as the microhardness value of each of the samples. Density measurements were carried out using an electronic densometer based on the Archimedes principle. The phase analysis of the well-mixed powders and consolidated samples was conducted using X-ray diffractometry, utilizing a PW1710 Philips, PANalytical Empyrean model while the microstructural characterization was achieved through an FE-SEM (JEOL JSM 7600 F) equipped with energy-dispersive capabilities.

3 Results and discussion

3.1 Predicted thermophysical values for the designed CuNbMnCrNiCo HEA

Thermophysical expressions depicted in Table 1 were used to design and predict or identify the phase(s) in the HEA used in this study. The predicted values obtained for the CuNbMnCrNiCo HEA developed in this study are shown in Table 4.

Table 4 Predicted values for the CuNbMnCrNiCo HEA used as reinforcement in the study

S/*N*	Parameters	Obtained values
1	Dimensionless parameter (Ω)	6.90
2	Atomic mismatch (δ)	5.53%
3	Mixing enthalpy (ΔH_{mix})	3.16 kJ/mol
4	Melting temperature of the HEA (T_{mix})	1535 °C
5	Mixing entropy (ΔS_{mix})	14.21 J/K
6	Valence electron concentration (*VEC*)	8.20

3.2 CALPHAD phase prediction for HEA

In the pursuit of understanding the phases present in the HEA used as reinforcement in metal matrix composites, the calculation phase diagram (CALPHAD) software, specifically Thermocalc, emerged as a powerful tool. Leveraging the TCHEA2 database during phase prediction, the software generated valuable insights as depicted in Fig. 3. Given the sintering temperature constraint of the HEA-reinforced Al matrix composite (which is 520 °C, below 600 °C), this study focuses on identifying phases within this temperature range. Thermocalc indicated that body-centered cubic (BCC), face-centered cubic (FCC), and Laves phases were potential constituents of the HEA at the sintering temperature, as illustrated in Fig. 3. These predicted phases offer crucial expectations for the microstructure of the sintered HEA-reinforced Al matrix composites.

The results obtained from the CALPHAD prediction software offer valuable insights into the phase evolution of the designed HEA across a temperature range. At temperatures from 0 to 400 °C, the CALPHAD prediction identifies three primary phases: FCC_L12, BCC_B2, and C14_Laves. FCC_L12, with its face-centered cubic structure, is anticipated to be the dominant phase at lower temperatures due to its favourable packing efficiency and high configurational entropy. Concurrently, BCC_B2 and the intermetallic C14_Laves phase may coexist, with the latter present in trace amounts, particularly rich in Nb.

As the temperature escalates from 400 to 700 °C, the CALPHAD prediction indicates a diminishing mole fraction of FCC_L12, with BCC_B2 and C14_Laves phases gaining stability. Around 700 °C, BCC_B2 and C14_Laves might surpass or equate the abundance of FCC_L12. Focusing on the specific sintering temperature of 520 °C for the designed

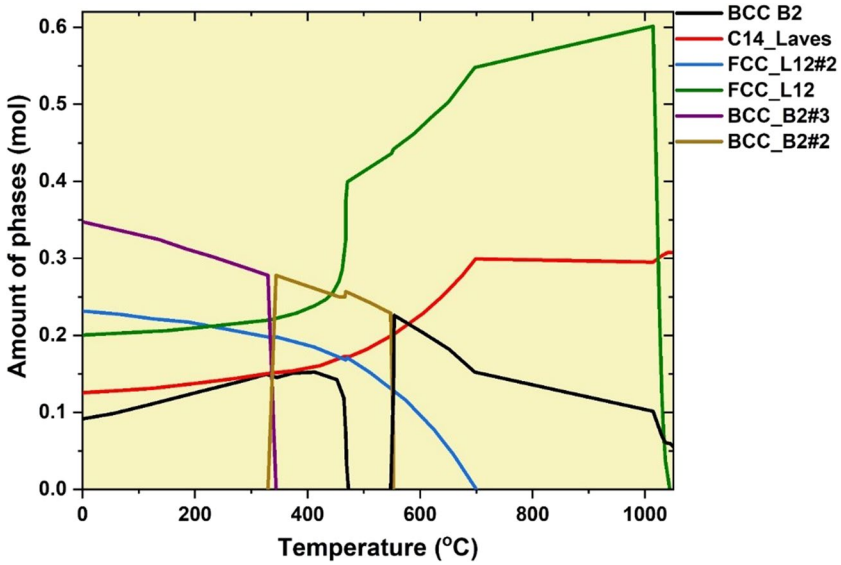

Fig. 3 CALPHAD stable phase prediction for HEA

HEA, CALPHAD suggests a blend of FCC_L12 and BCC_B2 phases, possibly accompanied by a minor presence of C14_Laves. Actual phase fractions will depend on variables like cooling rate and microstructural details.

It is worth noting that CALPHAD prediction aligns with the valence electron concentration (VEC) value obtained, as demonstrated in Table 4. The calculated VEC value of 8.20 suggested that the FCC phase is more stable in the developed HEA at the sintering temperature considered. This alignment between theoretical VEC calculations and CALPHAD predictions buttresses the reliability of the VEC approach. Importantly, this approach finds concurrence in previous studies employing CALPHAD software for confirming VEC calculations and identifying phases in HEA [28, 29]. The synergy between experimental results and CALPHAD predictions enhances our understanding of the microstructural landscape of HEAs, contributing to the precision and efficacy of alloy development strategies.

3.3 Microstructures

The scanning electron microscopy (SEM) micrographs offer valuable insights into the morphological characteristics of powdered samples, unravelling the influence of the HEA additions to pure Al. In the micrograph of pure Al powder Fig. 4a (i), a predominantly uniform distribution of spherical particles is evident, showcasing minimal variation in size and shape. The smooth surface texture suggests effective processing with limited agglomeration or deformation, and the particles, ranging from a few to tens of microns in diameter, highlight a well-processed and homogeneous state [30].

Contrastingly, the SEM micrograph of milled HEA powder Fig. 4a (ii) unfolds a narrative of a wider particle size range and irregular shapes. Mechanical milling induces fragmentation, leading to angular features in some particles, and the rougher surface texture hints at the presence of surface features or debris from the milling process. These variations underscore the challenges in achieving complete homogeneity during milling. For the composite micrographs of 5%, 7%, and 10% HEA + Al Fig. 4a (iii, iv, v), the interface between Al and HEA phases remains distinct, revealing effective mixing with minimal visible interaction or diffusion. As HEA concentration increases, the microstructure suggests denser packing and potentially more interparticle contact, impacting both macro and microstructural properties [31, 32]. These observations collectively shed light on the complex interplay within HEA-reinforced Al matrix composites, providing critical insights into microstructural evolution and its implications for final material properties [32].

The X-ray diffraction (XRD) patterns for milled and mixed powders, comprising pure Al, high HEA, and HEA-reinforced Al matrix composites as indicated in Fig. 4b, reveal distinctive phase compositions. Pure Al exhibits clear peaks indicative of its single-phase face-centered cubic (FCC) structure with consistent positions. Milled HEA displays coexisting body-centered cubic (BCC) and FCC phases, along with the formation of the intermetallic compound Cr_2Nb, introducing complexity to its mechanical properties. The HEA-reinforced Al matrix composites exhibit concurrent peaks for Al, BCC HEA, FCC HEA, and Cr_2Nb, with increasing HEA content, thus correlating with higher relative intensities of HEA peaks.

In the SEM micrograph of spark plasma-sintered pure aluminium and its associated EDS mapping and elemental mapping (Fig. 5a (i–iii)), the well-controlled sintering process at 520 °C yields predominantly spherical particles with a uniform size distribution. The smooth surface texture indicates successful sintering without significant grain growth or agglomeration. The EDS mapping complements these findings, showcasing a uniformly bright green colour indicative of pure aluminium throughout the analyzed area. This uniformity suggests successful homogeneous sintering without localized segregation or impurities, thus emphasizing the effectiveness of the chosen parameters [33]. Overall, the combined SEM and EDS results affirm the successful production of dense and pure aluminium material with controlled morphology, thus setting the stage for promising mechanical properties [34], and the relatively short holding time of 10 min, along with the rapid heating rate of 100 °C/min, could have contributed to efficient densification [33].

The SEM micrographs and EDS mappings of 5 wt% (Fig. 5b (i–iii)), 7 wt% (Fig. 5c (i–iii)), and 10 wt% HEA-reinforced Al matrix composites (Fig. 5d (i–iii)) offer comprehensive insights into their microstructural evolution. In the 5 wt% HEA composite, the microstructure displays well-distributed and bonded HEA particles within the Al matrix. These particles exhibit irregular shapes and sizes, suggesting effective milling before sintering. The presence of lave phases at the HEA-Al interface implies potential interaction during sintering. EDS phase mapping and elemental mapping confirm a homogeneous HEA phase with distinct Al matrix and Laves phases, validating successful fabrication. For the sample with 7 wt% HEA composite (Fig. 5c (i–iii)), similarities with the 5 wt% HEA-reinforced composite are noted, as the composite displayed good dispersion and bonding of HEA particles. However, an increase in particle size and potential agglomeration is observed, likely attributed to the higher initial HEA content. The Laves phases in the 7 wt% HEA-reinforced Al matrix composite remain comparable in size and distribution to that with 5 wt% HEA, thus indicating that the increased HEA content does not significantly alter their formation. EDS mappings confirm a well-mixed and single-phase HEA, maintaining distinct Al matrix and Lave phases. In 10 wt% HEA composite (Fig. 5d (i–iii)), similarities persist with effective dispersion and

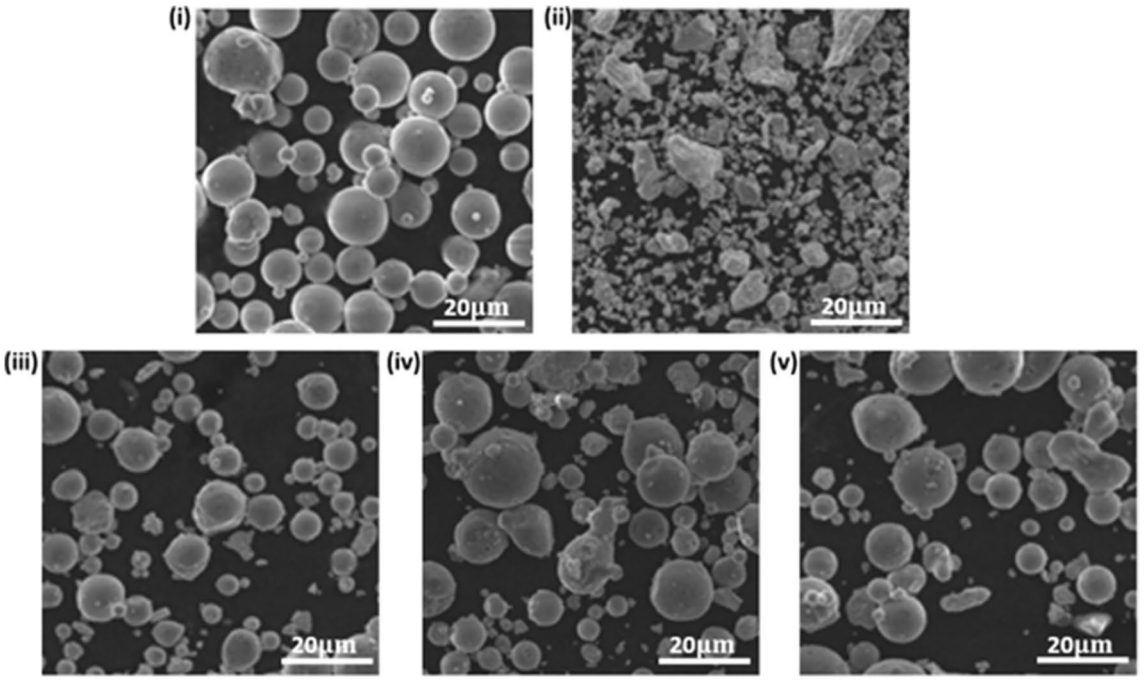

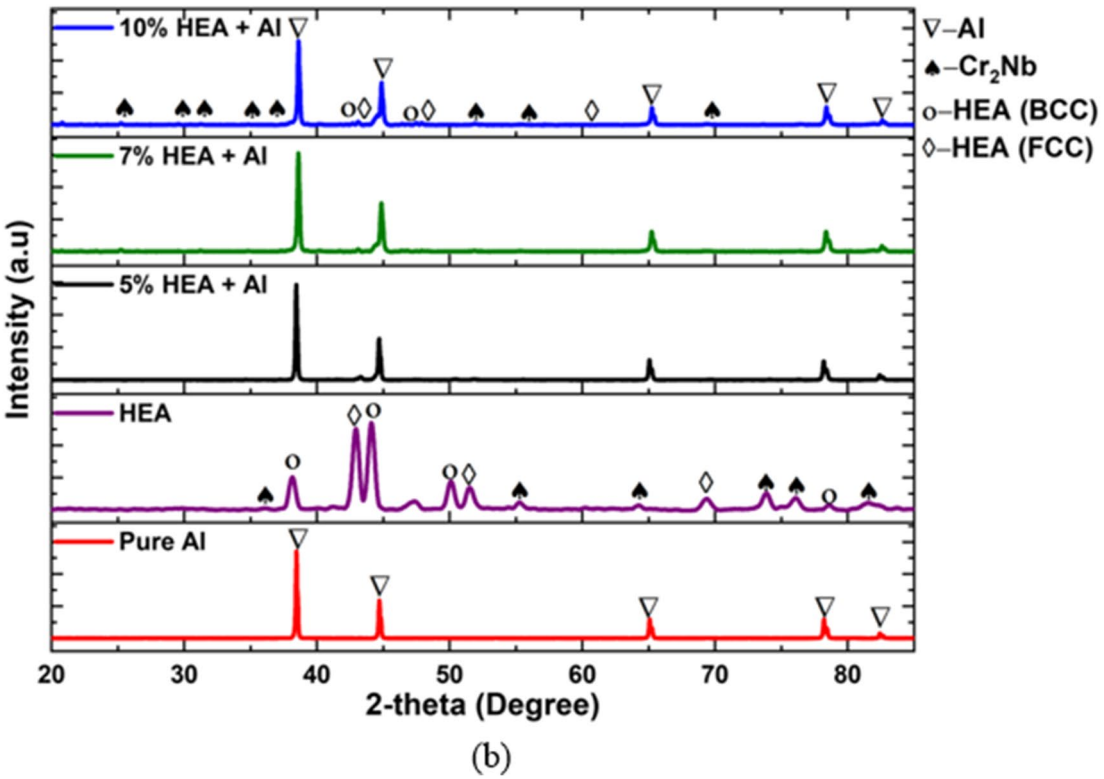

Fig. 4 Micrograph of **a** (i) pure Al powder, (ii) HEA (iii) 5 wt%, (iv) 7 wt%, and (v) 10 wt% HEA-reinforced Al powder. **b** XRD of the powders of (i)–(v)

bonding of HEA particles within the Al matrix. However, a noticeable increase in particle size and potential agglomeration is observed, emphasizing the impact of higher HEA content. Laves phases appear slightly larger and more frequent, thus indicating an influence from the increased availability of Nb and Cr. EDS mappings reaffirm a well-mixed

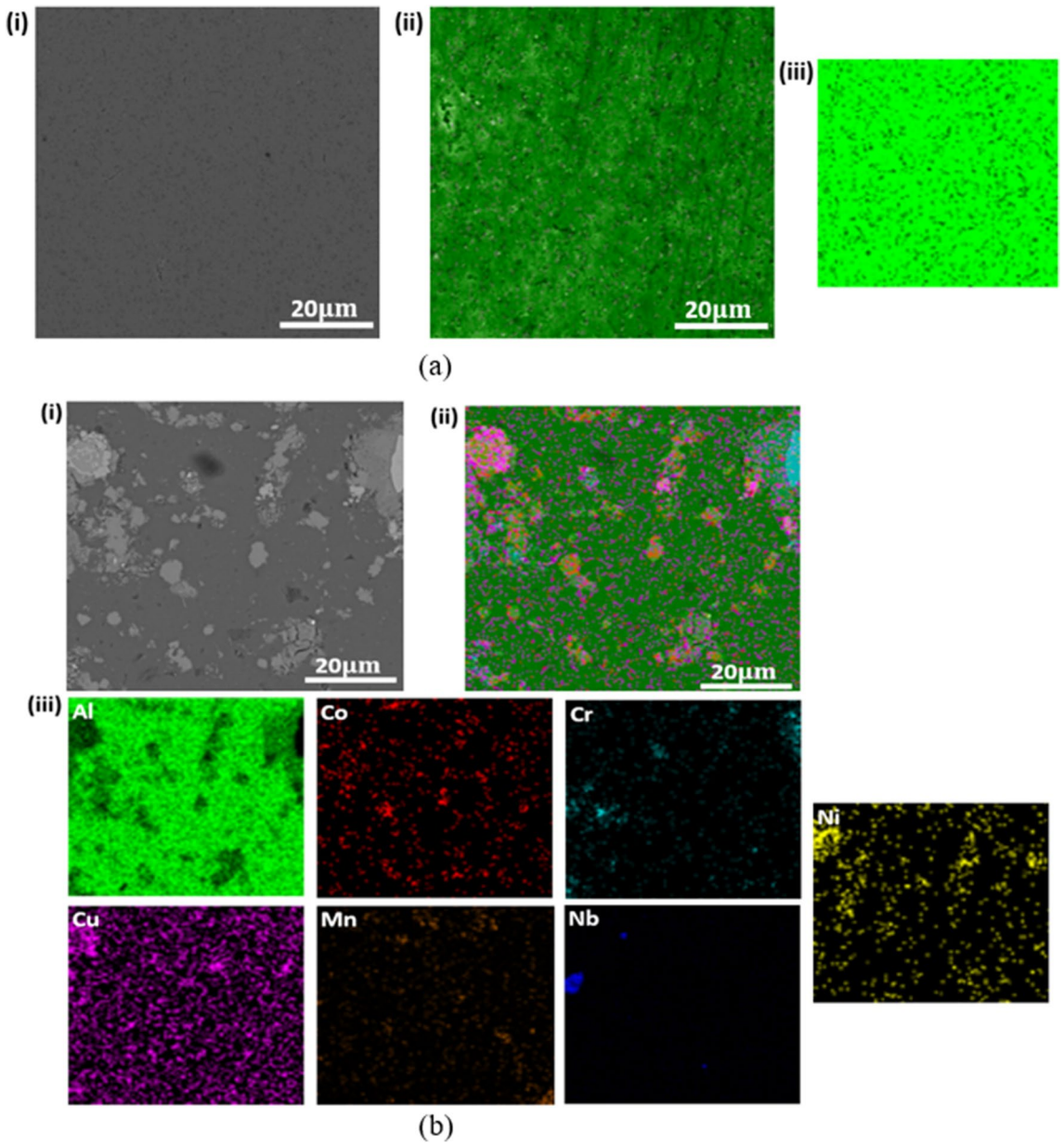

Fig. 5 **a** (i) SEM micrograph of sintered pure Al and their corresponding EDS phase and elemental mapping (ii–iii). **b** (i) SEM micrograph of sintered 5% HEA + Al and their corresponding EDS phase and elemental mapping (ii–iii). **c** (i) SEM micrograph of sintered 7% HEA + Al and their corresponding EDS phase and elemental mapping (ii–iii). **d** (i) SEM micrograph of sintered 10% HEA + Al and their corresponding EDS phase and elemental mapping (ii–iii). **e** XRD of sintered pure Al and HEA-reinforced Al. **f** Line scan EDS of 7% HEA-reinforced Al matrix composite at region of interdiffusion

and single-phase HEA, retaining clear distinctions between the Al matrix, HEA, and Laves phases.

Figure 5e shows the X-ray diffraction (XRD) analysis of field-assisted sintered samples. The figure elucidates the post-sintering crystalline characteristics and phase compositions of pure Al and HEA-reinforced Al matrix composites. For pure Al, the exclusive presence of FCC Al peaks and discerned peak intensities indicate its singular FCC crystalline structure. The observed peak intensities suggest potential grain growth resulting from the elevated-temperature sintering process. In the case of HEA-reinforced Al matrix composites, the concurrent appearance of peaks corresponding to Al, body-centered cubic (BCC) HEA, face-centered cubic (FCC) HEA, and Laves phases affirms the successful integration and dispersion of HEA particles within the Al matrix (citation). The rise in the relative intensities of HEA peaks with increasing HEA content underscores the adopted sintering technique's efficacy in achieving a homogenously

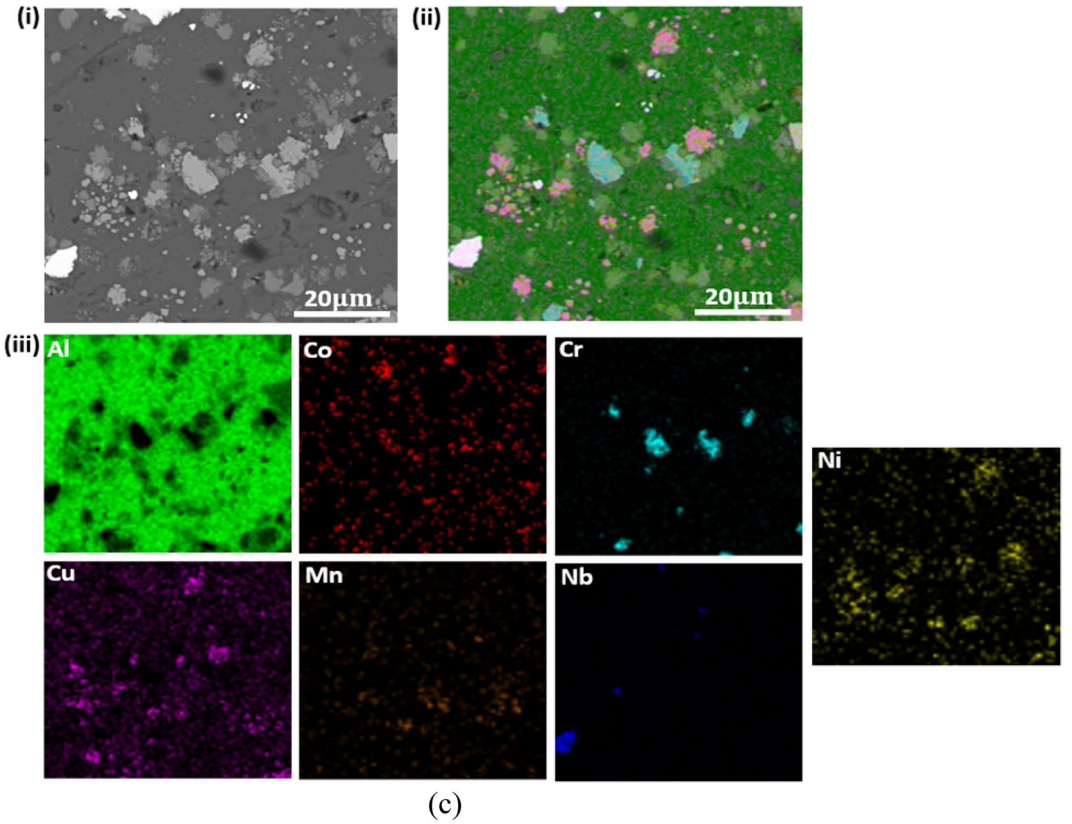

(c)

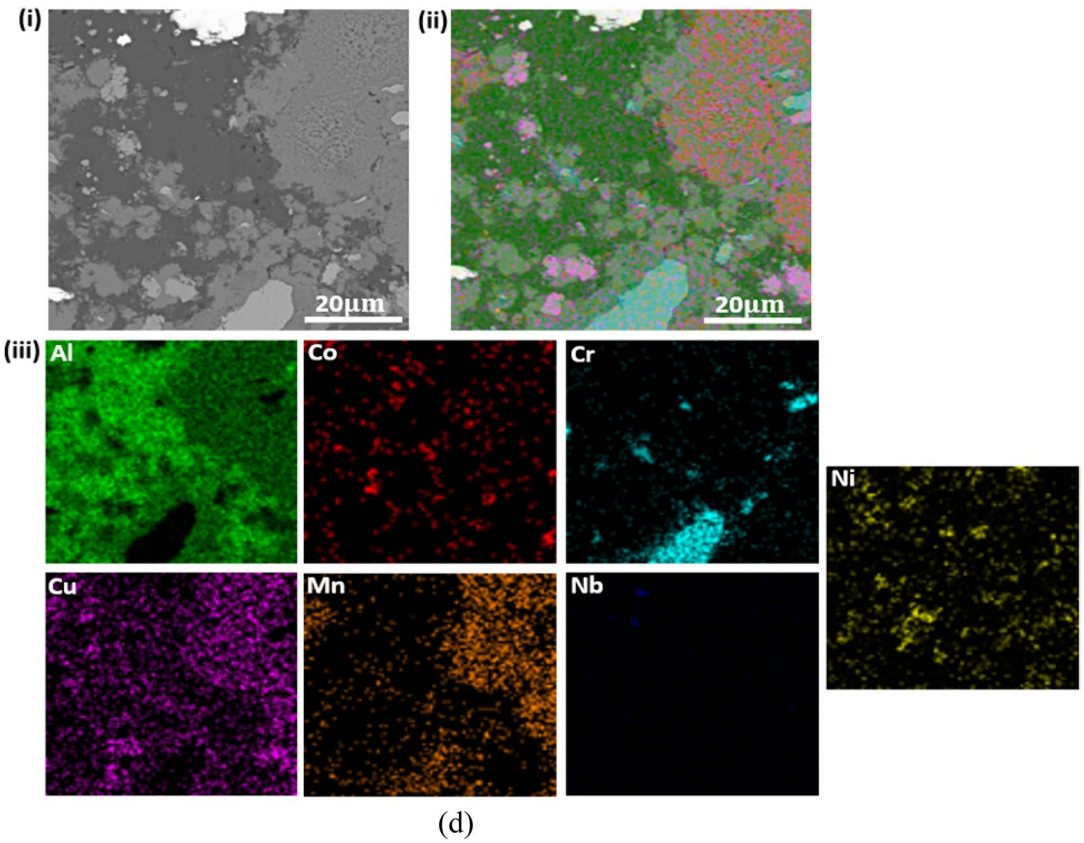

(d)

Fig. 5 (continued)

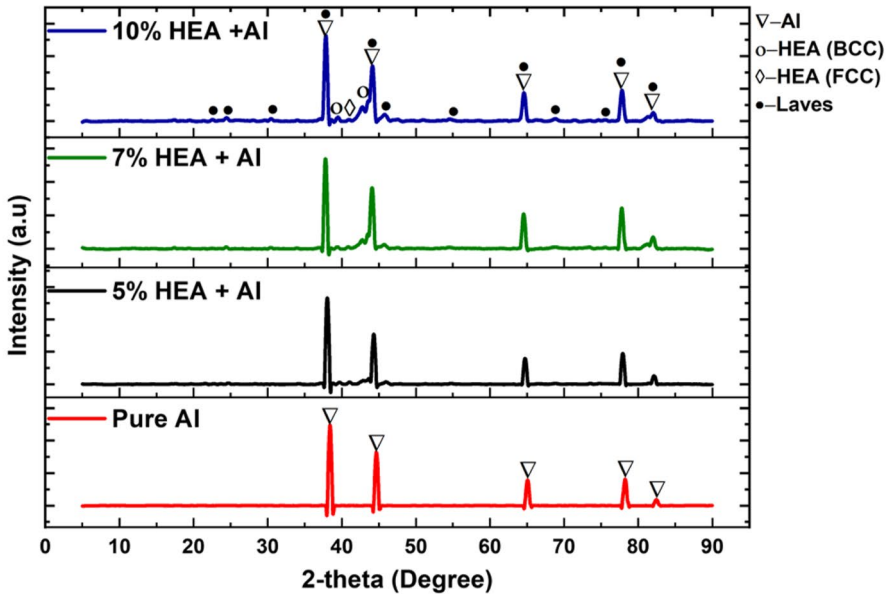

(e)

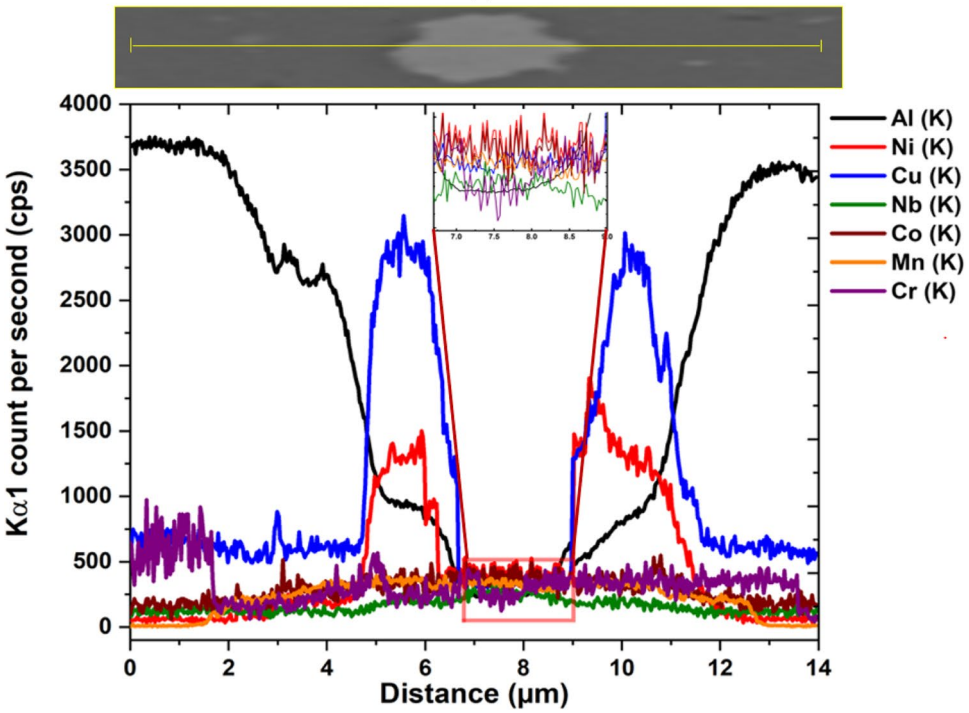

(f)

Fig. 5 (continued)

blended composite. The absence of novel peaks and sustained peak positions implies minimal interfacial reactions, ensuring the preservation of distinct phase properties and potential robust interfacial bonding between HEA and the Al matrix [35].

The EDS line scan of the field-assisted sintered HEA-reinforced Al matrix composite (Fig. 5f) yields crucial insights into the elemental distribution and interdiffusion dynamics within the material. A comprehensive representation of the plot shows distinct peaks for all HEA elements (Cu, Ni, Mn, Cr, Co, Nb) and Al, thus reflecting their incorporation into the composite. The varying intensities of these peaks along the scan line indicate localized

concentration differences and emphasize the heterogeneous composition of the material.

One notable feature is the well-defined interdiffusion zone observed between 6.8 and 9.0 µm. This region exhibits a relatively uniform distribution of elements, providing clear evidence of intermixing between the HEA and Al matrix. The gradual transition into and out of the interdiffusion zone, without abrupt spikes or drops in element concentration, suggests a controlled and nuanced diffusion process. This controlled diffusion is likely influenced by specific sintering parameters such as temperature, pressure, and holding time. Furthermore, within the interdiffusion zone, variations in peak heights for individual elements indicate subtle differences in concentration. These variations could stem from factors like atomic size discrepancies, element diffusivity, or preferential interactions during the sintering process [35].

3.4 Densification and microhardness

The influence of HEA addition on the microhardness and densification of the field-assisted HEA-reinforced Al matrix composites is depicted in Fig. 6. The unreinforced pure Al exhibited a microhardness of approximately 36.91 HV and a relative density of 98.9%, and the subsequent addition of HEA particles reveals intriguing trends. At 5 wt% HEA content, the microhardness increases to around 74.05 HV, signifying over a 100% enhancement compared to pure aluminium. Concurrently, the relative density experiences a slight reduction to about 98.8%, highlighting a subtle trade-off in density for increased hardness.

As the HEA content further rises to 7 wt%, the microhardness continues its upward trajectory to approximately 85.34 HV, representing about 131.2% increase from pure aluminium. Correspondingly, the relative density decreases to around 98.77%, emphasizing the continued inverse relationship between strength and density. Finally, at 10 wt% HEA content, the microhardness reaches approximately 107.41 HV, marking about 200% increase from pure aluminium. The relative density further decreases to about 98.60%, reinforcing the observed trade-off.

The observed increase in microhardness is rationalized by the superior hardness of HEA particles compared to the aluminium matrix. This strengthening effect is complemented by the HEA particles acting as effective barriers to dislocation movement, contributing to the overall reinforcement of the material [36]. Conversely, the reduction in relative density is attributed to the increased mass of HEA particles, causing a decline in overall composite density. These findings underscore the potential of HEA particles for substantial strength improvement in aluminium matrix composites but also highlight the inherent compromise between strength, density, and material brittleness.

4 Conclusion

This study presents a comprehensive investigation into the design, phase identification, and microstructural properties of HEA-reinforced Al matrix composites. Both theoretical and experimental approaches were utilized to unravel the intricacies of HEA design, through the use of thermophysical expressions and calculation of phase diagram (CALPHAD) predictions. The presence of both BCC and FCC stable phases in the designed HEA predicted by the thermophysical expressions calculations aligns with the CALPHAD prediction experimental results from scanning electron microscopy

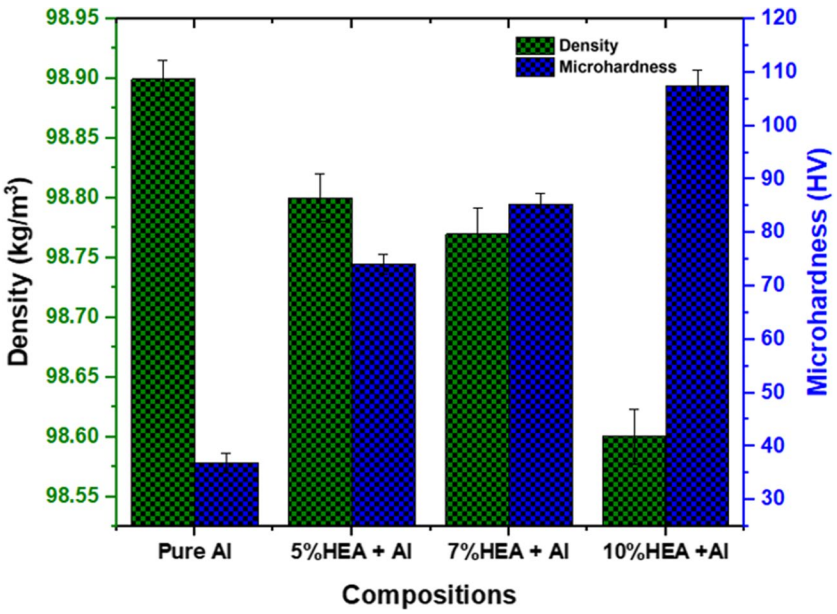

Fig. 6 Densification and microhardness of field-assisted sintered pure Al and HEA-reinforced Al matrix composites

(SEM) micrographs and X-ray diffraction (XRD) analyses offered valuable insights into the microstructural evolution of HEA-reinforced Al matrix composites, showcasing fair dispersion, bonding, and phase integration.

The EDS line scan emphasized the controlled interdiffusion dynamics within the composite, thus contributing to a nuanced understanding of compositional heterogeneity. Furthermore, the study demonstrated that the addition of as low as 5 wt% HEA particles significantly enhanced the microhardness of the Al matrix composites. Nevertheless, the densification results showcase a remarkable trade-off between increased microhardness and marginal reduction in density. The observed trends in microhardness and densification highlight the significant potential of HEA particles as effective reinforcements, with implications for applications requiring improved material strength. Overall, the synergy between theoretical predictions using the thermophysical expression and CALPHAD software and experimental validations provided a robust foundation for advancing the development and application of HEA-reinforced Al matrix composites.

Acknowledgements The authors acknowledge Global Excellence and Stature (GES 4.0) and the Centre for Nanoengineering and Advanced Materials, University of Johannesburg, South Africa, for their immense support.

Author contribution Smith Salifu: conceptualization, designing the experiment, performing the experiments, writing the original draft. Peter Apata Olubambi: provided the needed materials and editing of the original manuscript.

Funding Open access funding provided by University of Johannesburg.

Data availability Data will be made available upon request.

Declarations

Ethics approval Not applicable

Consent to participate Not applicable

Consent for publication All authors have read and agreed to publish the manuscript.

Competing interests The authors declare no competing interests.

References

1. Wang N et al (2020) Microstructure and properties of aluminium-high entropy alloy composites fabricated by mechanical alloying and spark plasma sintering. Mater Today Commun 25:101366
2. Wang H, Xie J, Chen Y, Liu W, Zhong W (2022) Effect of CoCrFeNiMn high entropy alloy interlayer on microstructure and mechanical properties of laser-welded NiTi/304 SS joint. J Mater Res Technol 18:1028–1037
3. Miracle DB, Senkov ON (2017) A critical review of high entropy alloys and related concepts. Acta Mater 122:448–511
4. Ghrib T (2015) Structural, optical and thermal properties of nanoporous aluminum. Thermochimica Acta 599:57–62
5. Gan YX, Dong J, Gan JB (2017) Carbon network/aluminum composite made by powder metallurgy and its corrosion behavior in seawater. Mater Chem Phys 202:190–196
6. Reddy PV, Kumar GS, Krishnudu DM, Rao HR (2020) Mechanical and wear performances of aluminium-based metal matrix composites: a review. J Bio-and Tribo-Corrosion 6(3):83
7. Mohanavel V, Periyasamy P, Balamurugan M, Sathish T (2018) A review on mechanical and tribological behaviour of aluminium based metal matrix composites. Int J Mech Prod Eng Res Devel 473–478
8. Chen W et al (2019) Effect of ball milling on microstructure and mechanical properties of 6061Al matrix composites reinforced with high-entropy alloy particles. Mater Sci Engineering: A 762:138116
9. Li J et al (2020) Friction stir processing of high-entropy alloy reinforced aluminum matrix composites for mechanical properties enhancement. Mater Sci Engineering: A 792:139755
10. Tan Z, Wang L, Xue Y, Zhang P, Cao T, Cheng X (2016) High-entropy alloy particle reinforced Al-based amorphous alloy composite with ultrahigh strength prepared by spark plasma sintering. Mater Design 109:219–226
11. Wang Y et al (2022) High entropy alloy reinforced aluminum matrix composites prepared by novel rotation friction extrusion process: microstructure and mechanical properties. Mater Sci Engineering: A 854:143789
12. Zhao YF, Wang YQ, Wu K, Zhang JY, Liu G, Sun J (2018) Unique mechanical properties of Cu/(NbMoTaW) nanolaminates. *Script Mater* 154:154–158
13. Karthik GM, Panikar S, Ram GDJ, Kottada RS (2017) Additive manufacturing of an aluminum matrix composite reinforced with nanocrystalline high-entropy alloy particles. Mater Sci Engineering: A 679:193–203
14. Liu Y, Chen J, Li Z, Wang X, Fan X, Liu J (2019) Formation of transition layer and its effect on mechanical properties of AlCoCrFeNi high-entropy alloy/Al composites. J Alloys Compd 780:558–564
15. Chen J et al (2015) Fabrication and mechanical properties of AlCoNiCrFe high-entropy alloy particle reinforced Cu matrix composites. J Alloys Compd 649:630–634
16. Lu T et al (2018) The influence of nanocrystalline CoNiFeAl0. 4Ti0. 6Cr0. 5 high-entropy alloy particles addition on microstructure and mechanical properties of SiCp/7075Al composites. Mater Sci Engineering: A 726:126–136
17. Zhang L et al (2018) Microstructure and property characterization of Al-based composites reinforced with CuZrAl particles fabricated by mechanical alloying and spark plasma sintering. Adv Powder Technol 29(7):1695–1702
18. Kumar KP, Krishna MG, Rao JB, Bhargava N (2015) Fabrication and characterization of 2024 aluminium–high entropy alloy composites. J Alloys Compd 640:421–427

19. Salifu S, Olubambi PA (2024) Effects of fabrication techniques on the mechanical properties of high entropy alloys: a review. Int J Lightweight Mater Manuf 7(1):97–121 2024/01/01/
20. Yang X, Zhang Y (2012) Prediction of high-entropy stabilized solid-solution in multi-component alloys. Mater Chem Phys 132(2):233–238
21. Guo S, Ng C, Lu J, Liu CT (2011) Effect of valence electron concentration on stability of fcc or bcc phase in high entropy alloys. J Appl Phys 109(10):103505
22. Pohan RM et al (2018) Microstructures and mechanical properties of mechanically alloyed and spark plasma sintered Al0.3CoCrFeMnNi high entropy alloy. Mater Chem Phys 210:62–70
23. Yang X, Zhang Y (2012) Prediction of high-entropy stabilized solid-solution in multi-component alloys. Mater Chem Phys 132:2–3
24. Wu M et al (2023) Investigation of mechanical properties and wear resistance of A2/B2 type medium-entropy alloy matrix reinforced with tungsten particles by In-Situ reaction. Metals 13(4):656
25. Kumar A, Gupta M (2016) An insight into evolution of light weight high entropy alloys: a review. Metals 6(9):199
26. Takeuchi A, Inoue A (2000) Calculations of mixing enthalpy and mismatch entropy for ternary amorphous alloys. Mater Trans 41(11):1372–1378JIM, vol
27. Yadav S, Biswas K, Kumar A (2019) Spark plasma sintering of high Entropy alloys. In: Cavaliere P (ed) Spark plasma sintering of materials: advances in Processing and Applications. Springer International Publishing, Cham, pp 539–571
28. Oke SR, Falodun OE, Bayode A, Anamu US, Olubambi PA (2023) Phase prediction, densification, and microstructure of AlCrFeNi(TiO2)x high entropy alloy composite fabricated by spark plasma sintering. J Alloys Comp 968
29. Anamu US et al (2023) Fundamental design strategies for advancing the development of high entropy alloys for thermo-mechanical application: a critical review. J Mater Res Technol 27:4833–4860 2023/11/01/
30. Akinwamide SO, Lesufi M, Akinribide OJ, Mpolo P, Olubambi PA (2020) Evaluation of microstructural and nanomechanical performance of spark plasma sintered TiFe-SiC reinforced aluminium matrix composites. J Mater Res Technol 9(6):12137–1214
31. Li Q et al (2021) The influence of AlFeNiCrCoTi High-Entropy Alloy on Microstructure, Mechanical properties and Tribological behaviors of Aluminum Matrix composites. Int J Metalcast 15(1):281–291
32. Luo K, Liu S, Xiong H, Zhang Y, Kong C, Yu H (2022) Mechanical properties and strengthening mechanism of Aluminum Matrix composites Reinforced by High-Entropy Alloy particles. Met Mater Int 28(11):2811–2821
33. Rengifo S, Zhang C, Harimkar S, Boesl B, Agarwal A (2017) Effect of WS 2 addition on tribological behavior of aluminum at room and elevated temperatures. Tribol Lett 65:1–10
34. Akinwamide SO, Maleka M, Motabeni N, Akinribide OJ, Oluwasegun FE, Olubambi PA (2023) Synthesis and characterization of spark plasma sintered zirconia and ferrotitanium reinforced hybrid aluminium composite. Int J Adv Manuf Technol 125(1–2):763–776
35. Yuan Z, Tian W, Li F, Fu Q, Hu Y, Wang X (2019) Microstructure and properties of high-entropy alloy reinforced aluminum matrix composites by spark plasma sintering. J Alloys Comp 806:901–908
36. Salifu S, Olubambi PA, Teffo L (2024) Phase stability and microstructural properties of high entropy alloy reinforced aluminium matrix composites consolidated via spark plasma sintering, Heliyon